GEOPHYSICAL RESEARCH LETTERS, VOL. 23, NO. 10, PAGES 1191-1194, MAY 15, 1996

Neon-20, Oxygen-16, and Helium-4 densities, temperatures, and suprathermal tails in the solar wind determined with WIND/MASS

Michael R. Collier,[1] D.C. Hamilton,[1] G. Gloeckler,[1] P. Bochsler,[2] and R.B. Sheldon[2]

Abstract. Measurements from the MASS instrument on the WIND spacecraft from late Dec. 94 through Aug. 95 are reported for ^{20}Ne, ^{16}O, and ^{4}He. The average ^{4}He/^{20}Ne density ratio is 566 ± 87 with considerable variability. The average ^{16}O/^{20}Ne density ratio is 8.0 ± 0.6 and is independent, within experimental uncertainty, of solar wind speed. The ^{20}Ne/^{4}He and ^{16}O/^{4}He temperature ratios at the lowest solar wind speeds are consistent with unity, increasing with increasing speed to values exceeding that expected from mass proportionality. ^{20}Ne, ^{16}O, and ^{4}He distribution functions exhibit high energy tails which are well-fit by a kappa function.

Introduction

The MASS instrument on the WIND spacecraft, a high resolution electrostatic mass spectrometer, has provided elemental and isotopic abundances, temperatures, charge state distributions, and reduced distribution functions extending well into the suprathermal tails for solar wind ions near 1 AU since becoming fully operational in late Dec. 1994.

In this paper, we report average solar wind ^{20}Ne, ^{16}O, and ^{4}He abundances and temperature ratios as a function of solar wind speed and give the distribution functions during the time period from Dec. 1994 through Aug. 1995.

MASS Instrument Operation

Particles entering the MASS sensor first pass through a spherical segment electrostatic deflection system that makes 60 logarithmically spaced voltage steps in 3.2 minutes, covering 0.52 to 9.89 keV/e with a 4% (FWHM) passband. Ions then enter the TOF spectrometer through a 2 μg/cm^2 carbon foil, creating secondary electrons for the start signal and changing the ion's charge state to predominantly 0 or +1. The harmonic retarding potential inside the spectrometer has the unique property that the ion time-of-flight is independent of the ion energy or entering angle and is proportional to the square-root of its mass per charge, or for +1 ions, simply its mass. Consequently, a measurement of the ion's time of flight, which in the MASS instrument is accurate to better than 1 ns out of typical times-of-flight from 60 to 400 ns, yields a very precise measurement of its mass ($m/\Delta m \sim 100$).

The MASS instrument divides the spacecraft spin into a 45° sun sector and a 315° non-sun sector. Only sun sector data were analyzed in this study. See Gloeckler *et al.* [1995] for a more detailed description of the MASS instrument and Hamilton *et al.* [1990] for more information on the high resolution TOF mass spectrometer.

[1] Physics Dept., Univ. of Maryland, College Park, U.S.A.
[2] Physikalisches Institut, Universität Bern, Switzerland.

Paper number 96GL00621
0094-8534/96/96GL-00621$05.00

Analysis Technique

Because ions traverse an energy per charge analyzer before entering the time-of-flight section of the instrument, MASS is capable of measuring basic solar wind properties such as the proton and helium convection speed without the aid of the spectrometer. This permits MASS data to be conveniently binned according to solar wind speed with the resultant spectra plotted as a function of ion speed divided by solar wind convection speed.

The data were collected in one day intervals. In order to be considered a valid day for analysis, three conditions had to be met: (i) the solar wind speed must have remained constant over the course of the day to within ±10%, (ii) at least 99% of the approximately 3.2 minute science records must have yielded a valid Gaussian fit to the unsectored TOF start counting rate that was used to determine the solar wind proton convection speed, and (iii) the instrument status must have been nominal throughout the entire day.

The first two acceptance criteria were necessary because the distribution functions are determined *in the frame of the solar wind*, taking into account changes in the solar wind speed over about 3.2 minute periods. Consequently, it is critical to have an accurate determination of solar wind speed throughout the analysis interval. The third acceptance criterion was necessary because, as a result of spacecraft maneuvers, rare DPU latch-ups, etc., the instrument status occasionally was not optimized for science.

Appropriate time-of-flight ranges were determined for ^{4}He, ^{16}O, and ^{20}Ne from calibration data. Two background time-of-flight ranges, one at low and one at high times-of-flight relative to the main peak, were used to subtract background, including any possible background gradient effects. The background-adjusted counts were then efficiency corrected using calibration data to determine distribution functions. Background corrections were a couple percent for helium, 5-20% for oxygen, and 25-60% for neon.

Distribution functions were generated by summing the data from all the one day periods falling into a given 50 km/s wide solar wind speed bin. The resultant distributions were fit to Maxwellian and, in the case of helium, kappa functions to determine densities and kinetic temperatures. Long averaging periods were necessary to generate adequate counts of the less-abundant ion species and may have introduced some unavoidable aliasing due to fluctuations. For example, a significant *random* convection speed difference between the protons and the minor ion species operating on a shorter time scale than the averaging would increase the apparent width of the distribution function resulting in an overestimate of the kinetic temperature of the species. However, variation in the solar wind convective speed alone will not affect the results, and no evidence has been found for such a random differential flow.

Figure 1 shows the ^{4}He kinetic temperature determined from the MASS instrument versus its convection speed. The solid line is a fit to the data from this study which yields $< T_{He} >^{1/2} = (0.076 \pm 0.005)U - (15.0 \pm 3.0)$ where T_{He}

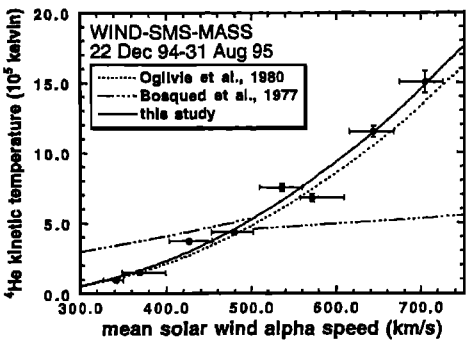

Figure 1. The observed ^{4}He kinetic temperature versus its convection speed.

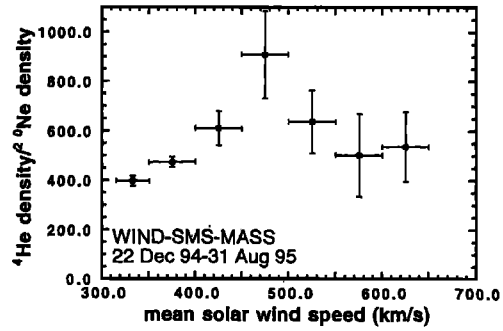

Figure 2. The ^{4}He/^{20}Ne density ratios as a function of solar wind speed.

is in kilokelvin and U in km/s. The dotted line reproduces a fit to ISEE-3 data published by Ogilvie *et al.* [1980]. The discontinuous dashed/dotted line represents the relationship determined by Bosqued *et al.* [1977] using Prognoz 1 data.

Density Ratios

Table 1 summarizes some of the results of this study. The data are grouped according to solar wind speed with each interval containing 8 to 27 days of data. The ^{16}O density includes both charge state +6 and +7 whereas the ^{20}Ne density includes charge state +8. Over the expected range of solar wind ionization temperatures, about 98% of the solar wind neon will be in charge state +8 and about 96% of the oxygen will be in charge states +6 and +7 [Arnaud and Rothenflug, 1985], so that ignoring other charge states of ^{20}Ne and ^{16}O will introduce an error of about 2% in the ratios.

Figure 2 shows the ^{4}He/^{20}Ne density ratio as a function of solar wind speed. At low solar wind speeds, the ^{4}He/^{20}Ne ratio increases with increasing solar wind speed although there appears to be significant temporal variability in this ratio [Kunz *et al.*, 1983], so that the possibility that the observed statistically significant changes in this ratio with solar wind speed may simply reflect this variability cannot be ruled out. However, if this trend is real, it resembles the trend seen in the He/H density ratio at these speeds [Neugebauer, 1981a,b, 1992] and suggests that the average Ne/H ratio does not vary much with solar wind speed between 315 and 500 km/s. At higher solar wind speeds, this ratio shows great variability, with values ranging from about 500 to about 900. The upward trend in this ratio established at low velocities does not extend beyond solar wind speeds of 500 km/s, suggesting that, because the He/H density ratio increases with increasing solar wind speed, even within coronal hole-type flow, the Ne/H ratio may also increase with increasing solar wind speed within this high speed regime.

The average ^{4}He/^{20}Ne ratio is 566 ± 87. Geiss *et al.* [1970] and Geiss *et al.* [1972], using foils placed on the moon during the Apollo missions, reported a ^{4}He/^{20}Ne flux ratio of 570 ± 70, consistent with the results of this study (see also Gloeckler and Geiss, 1989). Because the Geiss *et al.* [1970, 1972] results occurred near solar maximum in the declining phase of the solar cycle, and the results of this study are close to solar minimum, there does not appear to be any evidence for a solar cycle variation.

Kunz *et al.* [1983] determined He/Ne ratios for three periods in 1980. Their results yield a He/Ne abundance ratio of 518 ± 280, which, when corrected for a 7% ^{22}Ne contribution, gives a ^{4}He/^{20}Ne abundance ratio of 560 ± 300, consistent with the results of this study. Bochsler *et al.* [1986] later extended that study to include significantly more spectra and reported a He/Ne abundance ratio of 470 ± 150, which gives a ^{4}He/^{20}Ne abundance ratio of 510 ± 160, again consistent with the results of this study. The results reported here are of improved accuracy over the previous spacecraft measurements.

Shown in column 4 of Table 1 is the ^{16}O/^{20}Ne ratio. This ratio shows no statistically significant variation with solar wind speed and yields an average ratio of 8.0 ± 0.6. Table 2 compares the results of this study with previous studies determining the O/Ne abundance ratios conducted at various times over the past fifteen years. All time periods analyzed by Kunz *et al.* [1983] and Bochsler *et al.* [1986] to determine O/Ne abundance ratios are in slow speed solar wind (<400 km/s), whereas the time periods analyzed by Gloeckler *et al.* [1989] are during high speed streams when the AMPTE/CCE spacecraft was in the terrestrial magnetosheath. Geiss *et al.* [1994] analyzed data from both fast and interstream solar wind. The value quoted for our study has been adjusted for a 7% contribution from ^{22}Ne. No obvious solar cycle variation in this O/Ne density ratio, such as the solar cycle variation observed in the He/H density ratio [Neugebauer, 1981a,b], is apparent. However, if there is a small solar cycle variation [Feynman, 1983], it might be masked by instrument inter-calibration difficulties and differences in analysis techniques.

Table 1. Summary of the Results of This Study

speed (km/s)	days	$n_{^4He}/n_{^{20}Ne}$	$n_{^{16}O}/n_{^{20}Ne}$	$n_{^4He}/n_{^{16}O}$	$T_{^{20}Ne}/T_{^4He}$	$T_{^{16}O}/T_{^4He}$	$\kappa_{^4He}$
315-350	10	397 ± 20	7.9 ± 0.7	50 ± 4	1.04 ± 0.11	1.11 ± 0.13	$2.43^{+2.57}_{-0.19}$
350-400	27	473 ± 21	7.4 ± 0.6	63 ± 5	0.99 ± 0.08	1.06 ± 0.13	$2.68^{+0.38}_{-0.11}$
400-450	27	609 ± 69	8.2 ± 1.4	74 ± 10	2.52 ± 0.69	3.56 ± 0.82	$2.70^{+0.27}_{-0.11}$
450-500	12	908 ± 176	11.2 ± 3.2	81 ± 8	1.71 ± 0.79	5.46 ± 0.88	$3.23^{+0.63}_{-0.16}$
500-550	8	637 ± 127	7.7 ± 1.6	83 ± 10	3.07 ± 1.48	7.18 ± 0.76	$3.17^{+0.42}_{-0.18}$
550-600	8	502 ± 167	6.5 ± 2.3	79 ± 10	10.6 ± 6.50	6.52 ± 1.02	$3.93^{+0.85}_{-0.31}$
600-650	19	536 ± 141	7.5 ± 2.0	72 ± 6	10.4 ± 5.77	5.85 ± 0.57	$3.37^{+0.40}_{-0.22}$
650-700	10	—	—	62 ± 7	—	5.02 ± 0.81	$4.70^{+6.43}_{-0.93}$

Table 2. Comparison to the Results of Others

n_O/n_{Ne}	year	reference
6.3 ± 1.6	Jan80-Apr80	Kunz *et al.*, 1983
5.9 ± 0.7	Jan80-Apr80	Bochsler *et al.*, 1986
7.4 ± 0.6	Oct84-Nov84	Gloeckler *et al.*[1,3], 1989
9.9 ± 2.7	Aug92-Oct92	Geiss *et al.*[1], 1994
8.6 ± 2.9	Aug92-Oct92	Geiss *et al.*[2], 1994
7.4 ± 0.6	Dec94-Aug95	this study

1. fast streams; 2. interstream; 3. von Steiger *et al.*, 1996

Shown in column 5 of Table 1 is the ^{4}He/^{16}O density ratio. This ratio increases with increasing solar wind speed at low speeds similar to the ^{4}He/^{20}Ne density ratio. The average ^{4}He/^{16}O density ratio is 70 ± 7. consistent with the previously measured values 75 ± 20 by Bochsler *et al.* [1986] using data from the ISEE-3 spacecraft, and 66 ± 7 and 71 ± 17 by Villanueva *et al.* [1994] using data from the Voyager 1 and Voyager 2 spacecraft, respectively. Considering the increase observed in the He/H density ratio with increasing solar wind speed [Neugebauer, 1981a,b, 1992], it may be the case that the O/H and Ne/H density ratios do not vary much with solar wind speed over the range 315-500 km/s.

Kinetic Temperature Ratios

The sixth and seventh columns of Table 1 show the ^{20}Ne/^{4}He and the ^{16}O/^{4}He kinetic temperature ratios determined by Maxwellian fits to the distribution functions. The O^{+6} and O^{+7} temperatures are equal to within experimental uncertainties. The O^{+6} temperature is used in column six. The ^{20}Ne/^{4}He data are plotted in Figure 3.

A rough, empirically-derived relation for the kinetic temperature ratios T_i/T_j of two minor ion species of mass m_i and m_j in the solar wind is

$$T_i/T_j \approx m_i/m_j. \quad (1)$$

However, deviations from this relation are frequently observed [Ogilvie *et al.*, 1980; Bochsler *et al.*, 1985] and are generally attributed to dynamical effects in the solar wind. For example, the results of this study indicate that at low velocities, all ions appear to be in thermodynamic equilibrium, with temperature ratios of unity, perhaps as a result of collisions in interplanetary space [Kunz *et al.*, 1983]. Even up to average solar wind speeds (400-450 km/s), the ^{20}Ne/^{4}He and ^{16}O/^{4}He temperature ratios are significantly lower than those corresponding to equal thermal speeds (5 and 4, respectively) while increasing above these ratios at higher solar wind speeds. The data suggest that at the highest speeds at 1 AU the preferential heating of heavier ion species over lighter ion species occurs to a degree even greater than that given by equation (1).

The behavior of the neon to helium and oxygen to helium temperature ratios is similar to that reported for the alpha particle to proton temperature ratio which has also been observed to increase with increasing solar wind speed [Feynman, 1975] with a value that is correlated with the ratio of the solar wind expansion time scale to the hydrogen-helium equipartition time scale [Feldman *et al.*, 1974]. Furthermore, solar wind alpha to proton temperature ratios are frequently found to be in excess of four, which corresponds to equal thermal velocities [Neugebauer, 1976, 1981a].

Suprathermal Tails

Particle distributions exhibiting suprathermal tails that are well-fit by kappa functions have been observed throughout the heliosphere. The prevalence of this type of distribution suggests that a general principle, analogous to the central limit theorem for Maxwellians and applicable to diverse space plasma conditions, is necessary to adequately understand the origin of this extremely common distribution (see, for example, Collier [1993] and references therein.)

Figure 4 shows the distribution functions of ^{4}He, $^{16}O^{+6}$, and ^{20}Ne which were used, in conjunction with the $^{16}O^{+7}$ distribution function which is not shown, to generate the data in Table 1. The solid lines through each of the distributions in each of the three panels are Maxwellian fits to the data. The dotted lines through the helium data points in each panel show convected one dimensional kappa function fits to the data given by [Summers and Thorne, 1991]

$$f(v) = \frac{n\Gamma(\kappa+1)}{\omega_0\sqrt{\pi}\kappa^{3/2}\Gamma(\kappa-1/2)}\left[1+\frac{(v-v_c)^2}{\kappa\omega_0^2}\right]^{-\kappa}. \quad (2)$$

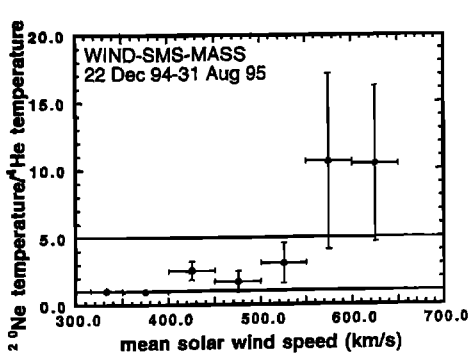

Figure 3. The ^{20}Ne/^{4}He temperature ratios as a function of solar wind speed.

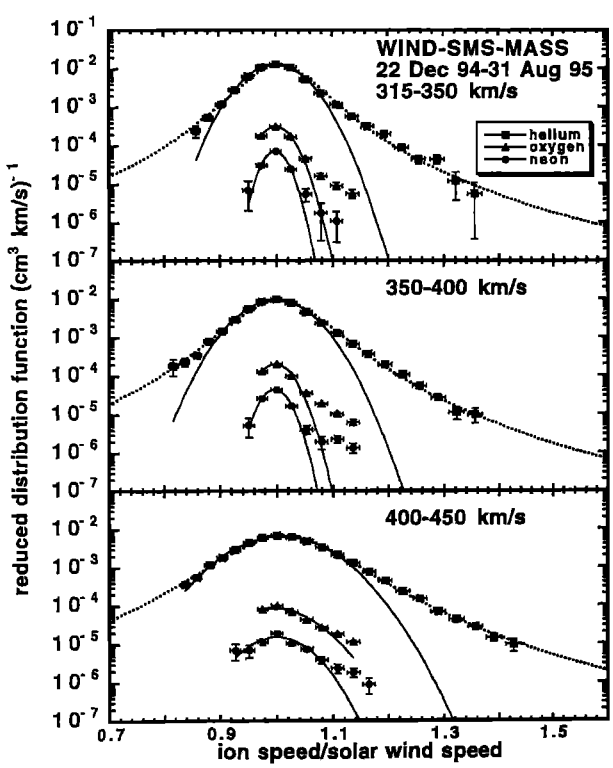

Figure 4. ^{4}He, $^{16}O^{+6}$, and ^{20}Ne solar wind distribution functions from the MASS instrument.

The density, n, core thermal speed, ω_0, and convective speed, v_c, inferred from the kappa function fits are usually identical, to within experimental uncertainties, to those inferred from the Maxwellian fit shown by the solid line. The kappa function, with its additional parameter, κ, which characterizes the high energy tail, fits the distribution accurately over the observed range of the data whereas the Maxwellian distribution characterizes only a small fraction of the entire distribution. These high energy tails are apparent in the distribution functions of the minor ion species ^{16}O and ^{20}Ne, as well.

The values of κ for the fits to the helium distribution functions are shown in column 8 of Table 1. The uncertainties on the value of κ were determined using the statistical uncertainties on the data points, generating fifty fictitious data sets, and using the distribution of the resultant κ-values. However, it is important to note that these values represent an average over many days of data. Averages over shorter, day long, time periods show significant variability, like that observed by Bosqued *et al.* [1977], although our average values of κ are consistent with those of Ogilvie *et al.* [1980]. The κ-values determined by averaging over many days of data increase with increasing solar wind speed or, equivalently, with increasing solar wind temperature, a trend that has been seen in a number of planetary magnetospheres [Collier and Hamilton, 1995].

Conclusion

^{20}Ne, ^{16}O, and ^{4}He abundance ratios, temperature ratios, and reduced distribution functions from the high resolution mass spectrometer MASS on the WIND spacecraft from late Dec. 94 through Aug. 95 have been reported. The average ^{4}He/^{20}Ne density ratio is 566 ± 87, but has significant variability with solar wind speed. The average ^{16}O/^{20}Ne ratio is 8.0 ± 0.6 with little or no variation evident with solar wind speed.

The ^{20}Ne/^{4}He and ^{16}O/^{4}He temperature ratios at low solar wind speeds are significantly lower than five and four, respectively, as would be expected if the distributions had equal thermal velocities, while increasing above these ratios at higher solar wind speeds. At the lowest velocities, the temperature ratios are consistent with unity.

^{20}Ne, ^{16}O, and ^{4}He distribution functions averaged over many days all exhibit high energy tails. The ^{4}He distribution function appears well-fit by a kappa function.

Acknowledgments. This research was supported by NASA under NAG52810 and by the Swiss National Science Foundation.

References

Arnaud, M. and R. Rothenflug, An updated evaluation of recombination and ionization rates, *Astron. Astrophys. Suppl. Ser., 60*, 425, 1985.

Bochsler, P. *et al.*, Kinetic temperatures of heavy ions in the solar wind, *J. Geophys. Res., 90*, 10,779, 1985.

Bochsler, P. *et al.*, Abundances of carbon, oxygen, and neon in the solar wind during the period from August 1978 to June 1982, *Solar Physics, 103*, 177, 1986.

Bosqued, J.M. *et al.*, Study of alpha component dynamics in the solar wind using the Prognoz satellite, *Solar Physics, 51*, 231, 1977.

Collier, M.R., On generating kappa-like distribution functions using velocity space Lévy flights, *Geophys. Res. Lett., 20*, 1531, 1993.

Collier, M.R. and D.C. Hamilton, The relationship between kappa and temperature in energetic ion spectra at Jupiter, *Geophys. Res. Lett., 22*, 303, 1995.

Feldman, W.C. *et al.*, The solar wind He^{2+} to H^{+} temperature ratio, *J. Geophys. Res., 79*, 2319, 1974.

Feynman, J., On solar wind helium and heavy ion temperatures, *Solar Physics, 43*, 249, 1975.

Feynman, J., Solar cycle and long term changes in the solar wind, *Rev. of Geophys. and Space Phys., 21*, 338, March 1983.

Geiss, J. *et al.*, Apollo 11 and 12 solar wind composition experiments: Fluxes of He and Ne isotopes, *J. Geophys. Res., 75*, 5972, 1970.

Geiss, J. *et al.*, Solar wind composition experiment, *Apollo 16 Preliminary Science Report, NASA SP-315*, 14-1, 1972.

Geiss, J. *et al.*, The neon abundance in the solar wind measured by SWICS on Ulysses, *EOS, Transactions, American Geophysical Union*, 75, 278, 19 April 1994.

Gloeckler, G. and J. Geiss, The abundances of elements and isotopes in the solar wind, *Cosmic Abundances of Matter*- C. Jake Waddington (ed.), pp. 49-71, AIP Conf. Proc. No. 183, Am. Inst. Phys., New York, 1989.

Gloeckler, G. *et al.*, Heavy ion abundances in coronal hole solar wind flows, *EOS, Transactions, American Geophysical Union*, 70, 424, 11 April 1989.

Gloeckler, G. *et al.*, The Solar Wind and Suprathermal Ion Composition Investigation on the WIND Spacecraft, *Space Science Reviews, 71*, 79, 1995.

Hamilton, D.C. *et al.*, New high-resolution electrostatic ion mass analyzer using time of flight, *Rev. Sci. Instrum., 61*, 3104, 1990.

Kunz, S. *et al.*, Determination of solar wind elemental abundances from M/Q observations during three periods in 1980, *Solar Physics, 88*, 359, 1983.

Neugebauer, M., The role of coulomb collisions in limiting differential flow and temperature differences in the solar wind, *J. Geophys. Res., 81*, 78, 1976.

Neugebauer, M., Observations of solar-wind helium, *Fund. of Cosmic Phys., 7*, 131, 1981a.

Neugebauer, M., Observations of solar-wind helium, *Solar Wind Four*, H. Rosenbauer (ed.), pp. 425-433, Report No. MPAE-W-100-81-31, Max-Planck-Institut für Aeronomie, Lindau, 1981b.

Neugebauer, M., Knowledge of coronal heating and solar-wind acceleration obtained from observations of the solar wind near 1 AU, *Solar Wind Seven*, E. Marsch and R. Schwenn (eds.), pp. 69-78, Pergamon Press, Oxford, 1992.

Ogilvie, K.W. *et al.*, Observations of the velocity distribution of solar wind ions, *J. Geophys. Res., 85*, 6069, 1980.

Summers, D. and R.M. Thorne, The modified plasma dispersion function, *Phys. Fluids B, 3*, 1835, 1991.

Villanueva, L. *et al.*, Voyager observations of O^{+6} and other minor ions in the solar wind, *J. Geophys. Res., 99*, 2553, 1994.

von Steiger, R. *et al.*, Composition of the solar wind, *Cosmic Winds and the Heliosphere*, J.R. Jokipii, C.P. Sonett, and M.S. Giampapa (eds.), in press, Univ. of Arizona Press, Tucson, 1996.

Michael R. Collier, D.C. Hamilton, and G. Gloeckler, Physics Dept., The University of Maryland at College Park, 20742.

P. Bochsler and R.B. Sheldon, Physikalisches Institut, Universität Bern, Sidlerstrasse 5, Bern, Switzerland.

(Received 31 October 1995; revised: 8 December 1995; accepted 19 January 1996)